Mejia John (Orcid ID: 0000-0001-6727-5541)
Nauslar Nicholas (Orcid ID: 0000-0003-1600-6311)

Impact of the North American Monsoon on wildfire activity in the southwest United States

Nicholas J. Nauslar[12], Benjamin J. Hatchett[1], Timothy J. Brown[1], Michael L. Kaplan[1], and John F. Mejia[1]

[1] Division of Atmospheric Sciences, Desert Research Institute, Reno, NV

[2]NOAA/NWS/NCEP Storm Prediction Center, Norman, OK

Corresponding author address: Nicholas J. Nauslar, 120 David L. Boren Blvd., Suite 2100 Norman, OK 73072-7304

Email: nick.nauslar@noaa.gov

Keywords: dry thunderstorms, fire management, fire weather, monsoon onset, self-organizing maps, synoptic classification

Abstract

The North American Monsoon (NAM) is an annual climate system phenomenon that develops over the Sierra Madre Occidental in western Mexico and spreads northward into the southwest United States from June through September bringing large quantities of rainfall and lightning, which can vary greatly on intra- and inter-annual time scales. The timing of the NAM onset can lengthen or shorten the wildfire season in the southwest United States. Here we determine NAM onset thresholds and subsequent dates for the Southwest Area (SWA; Arizona, New Mexico, west Texas, and Oklahoma panhandle) and each SWA Predictive Services Area (PSA) April through September from 1995-2013. Various wildfire activity thresholds were defined to capture days or events associated with increased wildfire activity that are considered 'busy' by wildland fire management in the context of an impact on firefighting resources. These defined thresholds allow for a unique examination of the relationship between the NAM and wildfire. Self-organizing maps (SOMs), utilizing 500 hPa geopotential heights and precipitable water, were implemented to identify atmospheric patterns contributing to the NAM onset and 'busy' days for the SWA and each PSA. Map types from the SOMs analysis showed the transition to, during, and from the NAM. Northward and eastward displacements of the subtropical ridge over the SWA were associated with NAM onset. Restructuring of the subtropical ridge in time (i.e., amplification or breakdown) as inferred from map types over the SWA was directly associated with increased wildfire activity. By identifying atmospheric patterns pertinent

to busy days of wildfire activity and a wildfire-based perspective of the NAM in the SWA, fire weather forecasters can proactively identify potential periods that may be particularly impactful on wildfire suppression resources.

1. Introduction

The North America Monsoon (NAM) affects much of North America with the largest impact in Mexico and the drylands of the southwest United States (hereafter Southwest; Figure 1a). The NAM is characterized as a large-scale atmospheric circulation that produces a distinct increase of warm-season (June through September) precipitation over North America (Adams and Comrie, 1997; Grantz *et al.,* 2007). The NAM core region is centered over the Sierra Madre Occidental in northwestern Mexico (Douglas *et al.,* 1993; Barlow *et al.,* 1998). It can extend into the Southwest and farther north into the western United States (Figure 1a)(Bryson and Lowry, 1955; Reiter and Tang, 1984; Tang and Reiter, 1984; Douglas *et al.,* 1993; Higgins *et al.,* 1999; Lo and Clark, 2002; Hawkins *et al.,* 2002). The variability of NAM in the southwestern United States is large, sometimes larger than the mean warm season rainfall, and is modulated by intraseasonal transient features including tropical easterly waves, tropical storms/cyclones, and transient upper-tropospheric troughs (Higgins *et al.,* 1998; Adams and Stensrud, 2007; Abatzoglou and Brown 2009; Hendon *et al.,* 2011; Means 2012; Favors and Abatzoglou, 2012; Newman and Johnson, 2012; Mejia *et al.,* 2015; Seastrand *et al.,* 2015; Pascale and Bordoni, 2016).

Higgins *et al.,* (1997) describe the NAM in three phases: development, mature, and decay. The development of the NAM (May–June) is characterized by a transition of generally westerly flow associated with a boreal winter circulation shifting to a southerly and easterly flow, and moves northward as the subtropical ridge develops over Mexico and

the Southwest (Bryson and Lowry, 1955; Adams and Comrie, 1997; Grantz *et al.,* 2007). The shift in winds is in response to surface heating over the continent, especially over the elevated terrain in the NAM region (Figure 1a). As the land-ocean temperature gradient increases, air flows towards the continent increasing convergence and enhancing the mountain-valley circulation over the Sierra Madre Occidental (Douglas *et al.,* 1993; Vera *et al.,* 2006; Grantz *et al.,* 2007; Gochis and Higgins, 2007). The pronounced diurnal cycle of rainfall associated with the NAM initially develops in southern Mexico before extending north to the Sierra Madre Occidental and the Southwest (June–July) (Douglas *et al.,* 1993; Adams and Comrie, 1997; Higgins *et al.,* 1997). The heaviest precipitation occurs in July and August during the mature stage then wanes in September (Carleton *et al.,* 1990; Douglas *et al.,* 1993; Higgins *et al.,* 1997). The NAM decay phase is more gradual than onset and represents the return to a cold season circulation with an equatorward migration of the polar jet stream. This transition is noted by a return of the westerlies from a diurnally driven, warm season circulation of easterly and southerly flow over the NAM region (Higgins *et al.,* 1997; Barlow *et al.,* 1998; Vera *et al.,* 2006; Cerezo-Mota *et al.,* 2011; Means, 2012).

There are several definitions for the NAM onset, but it is generally characterized by an increase of atmospheric humidity and precipitation associated with the establishment of the subtropical ridge over western Mexico and the Southwest (Adams and Comrie, 1997; Higgins *et al.,* 1997; Ellis *et al.* 2004; Grantz *et al.,* 2007). However, a universally accepted

NAM onset definition does not exist for the Southwest. NAM onset definitions include a dewpoint temperature of 54°F at the Tucson airport (National Weather Service Weather Forecast Office Tucson 2015), a precipitation threshold +0.5 mm day^{-1} for three consecutive days (Higgins *et al.,* 1997), or a Gulf of California sea surface temperature of 26°C (Mitchell *et al.,* 2002).

Limited research has examined the relationship between the NAM and wildfire occurrence in the western United States (Mohrle, 2003; Brandt, 2006; Evett *et al.,* 2008). In the Southwest, wildfire occurrence increases steadily through April, but the rate accelerates in May and June before decreasing in late July through September (Brandt 2006). The peak Southwest wildfire season occurs in June and early July due to decreasing fuel moisture, increasing temperatures, and enhanced ignition potential coinciding with drier thunderstorms before the NAM onset (Watson *et al.,* 1994; Westerling *et al.,* 2003). The NAM increases cloud-to-ground lightning, which increases "natural" wildfire ignitions, but with the corresponding increase in atmospheric and fuel moisture, wildfires often remain small as the NAM matures (Evett *et al.* 2008; Dowdy and Mills, 2012). The increase of cloud-to-ground lightning is related to 57% of natural wildfires that occur after NAM onset (Mohrle, 2003). Moreover, Mohrle (2003) notes 55% of large wildfires (40 hectares) and nearly 50% of area burned from large wildfires occur after onset demonstrating the delayed effects of NAM precipitation on fuel moisture recovery. However, wildfire occurrence abruptly decreases approximately midway through the climatological peak of

lightning and precipitation (late July to early August) in Arizona and New Mexico as fuel moisture rebounds (Hall 2007).

While a direct relationship exists between weather and wildfires, this relationship can be complex and nonlinear. Synoptic composites are often used to examine the relationships between the dominant atmospheric circulation systems and ecological factors (Hewitson and Crane, 2002). Self-organizing maps (SOMs) are utilized to identify atmospheric circulation patterns associated with different phenomena due to their propensity for objectively characterizing the complex distribution of synoptic states (Kohonen, 2001; Cavazos *et al.,* 2002; Hewitson and Crane, 2002; Crimmins, 2006; Reusch *et al.,* 2007; Reusch, 2011; Swales *et al.,* 2016). For example, Cavazos *et al.* (2002) showed that the NAM in southeast Arizona was dominated by three wet modes, while Crimmins (2006) identified different atmospheric patterns associated with extreme fire weather conditions in the Southwest.

Days with numerous wildfire ignitions and multiday wildfire events are of particular importance to fire meteorologists and managers due to the strain these events place on local, regional, and national suppression resources. Specifically, the Southwest Geographic Area Coordination Center, which oversees the coordination of firefighting resources in the Southwest Area (SWA) (Arizona, New Mexico, west Texas, and Oklahoma Panhandle) (Figure 1b) would bear the brunt of these impacts from these significant wildfire episodes or 'busy' days as fire management describes them. Identifying atmospheric patterns

pertinent to significant wildfire episodes in the SWA could provide improved prediction of significant wildfire episodes. This would facilitate more efficient allocation of firefighting resources during busy days.

In this analysis, we examine various definitions and thresholds for determining the NAM onset and significant wildfire episodes (busy days) within the SWA and its individual Predictive Services Areas (PSAs) (Figure 1b). We suggest that SOMs can help examine the intricate nonlinear relationships between the NAM and critical fire weather patterns leading to significant wildfire episodes. We implement SOMs to identify synoptic patterns that correspond to the NAM onset and significant wildfire episodes including those atmospheric patterns that are prevalent before, during, and after these events. SOMs help infer the associated physical climate processes between the NAM and wildfire activity.

2. Data

Data were collected for the SWA spanning April through September from 1995 to 2013 unless otherwise specified. Southwest Predictive Services defined the PSAs as having similar historical wildfire occurrences, fuel types, fuel indices, and climates (i.e., temperature and precipitation characteristics) (Figure 1b). They also determined large fire thresholds based on historical fire records and suppression needs (Table 1).

We used daily, 4 km surface gridded data of precipitation, minimum and maximum relative humidity (RH; RHmin; RHmax), specific humidity (q), minimum and maximum

temperature (Tmin; Tmax), and wind speed from the University of Idaho METDATA (Abatzoglou, 2013). Vapor pressure deficit (VPD) was defined as the difference between saturated vapor pressure and ambient vapor pressure. Saturated vapor pressure (e_s; in mb) was calculated using Teten's (1930) formula as follows:

$$e_s = 6.11 * 10^{((7.5*T)/(237.3+T))}$$

where T is temperature in °C. Vapor pressure deficit (VPD; in mb) was then calculated as:

$$VPD = e_s * RH/100$$

where RH is relative humidity in percent. A single daily PSA value for each variable was calculated by averaging all grid point values of each variable within a PSA.

Daily 700 hPa and 500 hPa winds, geopotential heights, and q and daily precipitable water (PW) were obtained from the National Center for Environmental Prediction (NCEP) North American Regional Reanalysis (NARR; Mesinger *et al.,* 2006) and downloaded from the Earth System Research Laboratory Physical Sciences Division (https://www.esrl.noaa.gov/psd/data/gridded/data.narr.html). Despite some known limitations of NARR (Dominguez *et al.,* 2008; Becker *et al.,* 2009; Cerezo-Mota *et al.,* 2011), numerous studies have shown NARR representative when examining synoptic circulation and moisture across the study region (e.g., Dominguez and Kumar, 2008; Dominguez *et al.,* 2008; Turrent and Cavazos, 2012; Doubler *et al.,* 2015; Radhakrishna *et al.,* 2015). We used a subset of daily NARR data that spanned from 85°W to 131°W longitude and 18°N to 49.5°N latitude.

Wildfire data were obtained from the Fire Program Analysis (FPA) quality controlled wildfire database (Short, 2015), which has the size, location, discovery date, ignition cause (i.e., type) among other information for each wildfire. Wildfires were categorized by type (all, lightning, human) and size (all, large) for each PSA, and large wildfire criteria were established from large wildfire thresholds determined by Southwest Predictive Services (Table 1). The Program for Climate, Ecosystem, and Fire Applications at the Desert Research Institute provided proprietary National Lightning Detection Network® CG lightning data.

3. Methods

3.1 The North American Monsoon Onset

The predictors selected for determining the NAM onset were the daily averaged PSA values of q, VPD, cloud-to-ground lightning strikes (LS), and precipitation. These variables were chosen because each represents atmospheric moisture or thunderstorm coverage, which are hallmarks of the NAM onset. To eliminate potential 'pre-monsoonal' moisture surges, time periods of three to ten days and variable thresholds that exceeded the 22-year, April through September PSA mean or median values for q and precipitation were considered. Periods where VPD values were less than their 22-year mean or median were also considered. A threshold of 100 LS was chosen due to the Storm Prediction Center using it as its forecast lightning density threshold and after examining various thresholds

between 25 and 200 LS. The primary technique for identifying NAM onset used six consecutive days of greater (less) than or equal to the 22-year median PSA value of q (VPD) and six consecutive days of at least 100 lightning strikes occurring concurrently (Onset1). Other combinations of variables were evaluated that substituted precipitation for q (Onset2) or VPD (Onset3). The NAM onset date for each PSA was determined by taking the first instance that met the Onset1, Onset2, or Onset3 requirements after 31 May. We constrained the onset after 31 May to minimize the influences of spring storms and also pre-monsoon moisture surges. While noting the subjectivity of these methods, they do represent the fundamental weather and climate shift the NAM exerts on the SWA and produces realistic results based on operational fire weather forecaster experience. For each PSA, the 10th percentile, 90th percentile, median, inter-quartile range, and +/- 1 median absolute deviation onset dates were calculated.

3.2 Significant Wildfire Episodes

The FPA wildfire occurrence data were organized by PSA and separated into categories based on size and type. If a day exceeded the 95th (99th) percentile for number of wildfires and large wildfires or at least two (three) large wildfires occurred for a PSA, it was considered a 'busy day' and exceeded the Busy95_PSA (Busy99_PSA) threshold. If a day exceeded the 95th (99th) percentile for number of large wildfires for the SWA, it was considered a 'busy day' and exceeded the Busy95_SW (Busy99_SW) threshold. Periods of

two, three, seven, and ten days that exceeded the 95th and 99th percentiles for large wildfires for the SWA over those respective time periods were identified as 'busy events'. These thresholds and periods represent a level of fire activity that can begin to stress local and regional wildfire suppression resources. The busy days and events were examined primarily to determine: 1) when these episodes occurred most frequently; and 2) to examine synoptic patterns during significant wildfire episodes (i.e., busy days or events).

3.3 Self-Organizing Maps

As noted in the introduction, SOMs are a nonparametric analysis technique based on neural networks that extract generalized patterns from gridded data defined over a region (Kohonen, 2001). SOMs can process multivariate, multidimensional input on a user-defined grid (e.g., 4x3; 12 nodes) by creating a spatially organized set of generalized patterns of variability from the input data (Reusch *et al.,* 2007; Reusch, 2011). SOMs capture the most notable atmospheric circulation patterns. Because the analysis is performed over daily time increments, such patterns include those modes related to synoptic scale variations (Cavazos *et al.,* 2002; Reusch *et al.,* 2007). This process is iterative and continues until the node locations and densities converge on a solution and become stable (i.e., stop changing) (Hewiston and Crane, 2002). The iterative SOMs process clusters nodes in regions where there is more information while spanning the distribution of data and placing similar (dissimilar) nodes closer to (farther from) each other (Hewistson and Crane, 2002). The

SOMs divide a continuum of atmospheric patterns into a small number of categories, which are spatially organized by similarity with similar patterns closer to each other and dissimilar patterns further away from each other on the user-defined grid (Hewitson and Crane, 2002; Reusch, 2011). By identifying atmospheric circulation patterns, SOMs allows a frequency analysis of each pattern, preferred transitions, and the ability to associate patterns with events (Cavazos *et al.,* 2002; Reusch *et al.,* 2007).

Although we did initially examine results using principal component analysis and k-means clustering, the SOMs methodology was ultimately chosen because it has been shown to be more robust, accurate, and able to provide better discriminating power of variability patterns in large, nonlinear datasets (Reusch *et al.,* 2007). Furthermore, SOMs allows more discrimination among subtle variations of similar atmospheric patterns (Hewitson and Crane, 2002). Kohonen (2001), Hewitson and Crane (2002), Reusch *et al.* (2007), and Reusch (2011) provide further detailed explanations of SOMs and the implementation of SOMs for meteorological and climatological applications.

SOMs was implemented using various packages from the Neural Network Toolbox in MATLAB© (Mathworks 2017). The input data consisted of standardized daily values of NARR 500 hPa geopotential heights, 700 hPa geopotential heights, and PW on a 175x120 grid (85°W-131°W; 18°N-49.5°N) for 183 days (1 April – 30 September) over 22 years (1992-2013). SOMs require standardized data when using multiple variables with varying scales (Reusch *et al*., 2007; Reusch, 2011). All input data was included together for training

because the primary goal of SOMs is to use generalized patterns determined from the input data as recommended by Reusch (2011). Asymmetrical grid configurations of nodes are recommended (Kohonen, 2001; Reusch *et al.,* 2007) thus node grid arrays of 4x3 (rows by columns), 5x3, and 4x5 were examined at 500, 1000, 2000, and 4000 iterations or until there was little variation of node densities and locations (i.e., stable). Sammon maps of multidimensional data on the different SOMs grids (not shown) and matching the input data to the final reference nodes of these grids displayed how dissimilar the nodes were and the distances among those nodes (Figure 2) (Sammon, 1969; Reusch *et al.,* 2007). Plots of neighbor node distances and examining the dates associated with each node were also helpful in examining the SOMs solutions (Figure 2). Each node was assigned a number (1-20) via SOMs, which helped facilitate analysis of the solutions. After a stable solution was reached, each day was classified with a node as a best match, which was composited into a map type (MT) for a particular meteorological variable (Reusch, 2011). After each day was classified, a frequency analysis was applied to all days, busy days/events, and onset days where applicable to determine if individual MTs or MT transitions were more associated with certain types of events.

4. Results

4.1 Atmospheric Map Types and NAM "Life Cycle"

The Sammon maps and neighbor node distances and densities for the three examined node grid configurations were all generally acceptable. Each grid configuration satisfied recommended SOMs mathematical requirements and resolved expected atmospheric patterns for the study area during the examined period (e.g., Hewitson and Crane 2002). However, the 4x5 grid resolved two patterns corresponding to busy and NAM onset days that were not well represented by the 4x3 and 5x3 grids. The 20 node configuration versus the 12 or 15 node configuration helped discriminate relatively subtle variations in the atmospheric circulation patterns especially at the intersection of troughs and ridges, which helped identify these two additional important MTs.

A stable solution was reached after 2000 iterations on the 4x5 SOMs grid, but the 4000 iteration version was utilized due to the slightly better coverage and shape from the Sammon map depiction (not shown). Figures 3-4 display the resulting twenty composite MTs from the SOMs analysis. Map Type 1 (MT {1}, e.g., Figure 3 {1}) for 500 hPa geopotential heights directly corresponds to MT {1} for both 700 hPa geopotential heights (not shown; similar to 500 hPa patterns) and PW (e.g.., Figure 4 {1}) because all three variables were included in the same SOMs analysis. Anomaly MTs were created, but as they were very similar in appearance, they are not shown here.

Each MT represents a node from the SOMs solution using the 4x5 grid with 4000 iterations. Figure 2 displays the distances (e.g., magnitude of dissimilarity) among adjacent nodes, and each one of those nodes corresponds directly to the MTs in Figures 3-4. For

example, the node at the very top, left of Figure 2, directly corresponds to MT 1. The number assigned to each node increases left to right across the columns and top to bottom across the rows. This layout helps compare the nodes/MTs mathematically and meteorologically.

Ascending numbered MTs follow a general progression of increasing geopotential heights and PW (Figures 3-4) {1-20}. Tighter geopotential height gradients, deeper troughs with lower heights, and drier conditions are illustrated at lowered numbered MTs (Figures 3-4 {1-10}) over the SWA and are most frequent in April and May (Table 2). Ascending numbered MTs generally occur in roughly chronological order through August. This trend parallels the amplification of subtropical ridge and increased moisture over northwestern Mexico and the SWA, which is indicative of the NAM (Figures 3-4; Table 2) (e.g., Douglas *et al.,* 1993; Adams and Comrie 1997). As the NAM decays in September, lower numbered MTs become more frequent indicating a decrease in geopotential heights and drier conditions (Figures 3-4 {12-13}).

April is characterized by deeper troughs and dry conditions prevailing across the SWA (Table 2; Figures 3-4 {1-2, 5-6}). The most prevalent MTs in May depict various longitudinal extents of the subtropical ridge axis that extends from the south and east over Mexico and the Gulf of Mexico (Table 2; Figure 3 {7-10}). Drier conditions remain over most of the SWA, but PW increases on the western and eastern coasts of Mexico (Figure 4 {7-10}). Geopotential heights continue to increase and the variation between troughs and

ridges over the SWA maximizes during June (Table 2; Figure 3 {8, 11-13}). In June, the subtropical ridge axis is centered over western and northwestern Mexico and PW increases in extent and magnitude across Mexico, the Plains, and the SWA (Figures 3-4 {11-13}; e.g., PSAs 13, 14N, 14S). The increase in lower-tropospheric moisture from the Gulf of Mexico is due in large part to the Low-Level Jet (Stensrud 1996; Higgins *et al.* 1997). During July, the transition to a ridge-dominated atmospheric pattern is complete with the establishment of the Four Corners High {i.e., MT 20}. This pattern continues through August with easterlies shifting northward bringing ample moisture across much of Mexico and into the SWA (Table 2; Figures 3-4 {15-16, 18-20}). In September, the subtropical ridge becomes less amplified with MTs demonstrating weaker ridges and troughs over the Southwest (Figure 3 {12-13, 17}).

The four most frequent MTs (Figure 3 {e.g., 16, 18-20}) show the SWA under the influence of the subtropical ridge, which is expected during the NAM (Adams and Comrie, 1997; Higgins *et al.,* 1997). PW increases in magnitude and northward extent during ridging confirming prior research (Figures 3-4) {e.g., 15-16, 18-20} (Carleton *et al.,* 1990; Higgins *et al.,* 1999; Cerezo-Mota *et al.,* 2011). Lightning strikes also increase during these ridging patterns. MTs {16, 20} have the highest median lightning decile (Table 2) and MTs {16, 19-20} are most associated with days exceeding the 70th percentile of LS across the SWA.

4.2 Quantifying NAM onset by Predictive Services Area

Figure 5 and Table 3 provide the median onset date, inter-quartile range, median absolute deviation, 10th percentile onset date, and 90th percentile onset date by PSA for the three onset metrics implemented. Onset1 (q, VPD, and lightning) and Onset2 (VPD, precipitation, and lightning) generally produce the same results with some variation across eastern New Mexico and west Texas (Figure 5). Onset3 (q, precipitation, and lightning) uniformly shows earlier median onset dates for every PSA except PSA SW14N (Figure 5), and Onset3 is less temporally variable than Onset1 and Onset2 (Table 3). Most onset dates for all the metrics occur in early to mid-July with a few instances of late June onset dates in some of the eastern New Mexico and west Texas PSAs (Figure 5). Depending on the PSA and metrics, the inter-quartile range can range from 10 to 53 days although most inter-quartile ranges total less than 35 days (Table 3). The median absolute deviations for onset are generally between one to two weeks with a few exceptions totaling around three weeks. The 10th and 90th percentile onset dates are generally separated by three to six weeks (Table 3), which indicates that while NAM onset varies interannually, it typically begins between late June and early August. Adjacent PSAs tend to have onset dates within a week of each other and occasionally on the same day.

Ridging, including a northward displacement of the subtropical ridge, southerly and easterly flow (inferred from assuming geostrophic flow at 500 hPa), increased moisture, and LS are associated with onset days (Figures 3-4) {15-16, 18-20} (Table 4). MTs {15-16,

18-20} total 28.7% of all days examined, but occur on 75.0% of onset days (Table 4). MTs {1-7} are never associated with onset for a PSA. These MTs generally depict lower heights and a trough at 500 hPa with less LS and drier conditions over the SWA. In these cases, moisture advection is limited from the eastern Pacific due to cooler waters and numerous mountain ranges between the Pacific and the SWA (Table 4) (Figures 3-4 {1-7}). These MTs also predominantly occur in April and May and rarely in June through August (Table 4).

4.3 Wildfire Occurrence Patterns and Associated Map Types

Annually, 51.5% of wildfires are human caused, but 57.2% of all large wildfires are lightning caused (Table 5). Wildfires increase in frequency into July before declining, confirming prior results from Brandt (2006). Seasonally, 3.5% of wildfires ignited in April through June become large, while only 1.9% of wildfires become large in July through September (Table 6). This finding is consistent with results from Mohrle (2003), who showed 57% of natural wildfires, but only 37% of total area burned from natural wildfires occurred after onset (early to mid-July). Human-related wildfires drop after onset also confirming findings from Mohrle (2003).

More than half of the days that exceeded the Busy95_PSA or Busy99_PSA threshold occurred before 1 July, and more than 82% of days that exceeded these thresholds occurred before the respective PSA's annual NAM Onset1 date (Table 7). When examining the entire Southwest, most of the busy days occur before 1 July and almost all of them

occur before August (Table 7). PSAs SW06S, SW08, and SW12 frequently had large fires when the Busy95_SW and Busy99_SW thresholds were exceeded (Table 8). On average, four PSAs had at least one large fire when exceeding the Busy99_SW threshold indicating widespread wildfire activity across the SWA during the busiest events.

MTs {4, 11-12, 16, 19-20} are most associated with days exceeding either the Busy95_SW or Busy99_SW threshold (Table 4). MTs {4, 11-12} are more associated with days exceeding either busy threshold than Onset1 days, while the converse is true for MTs {16, 19-20} (Table 4). Crimmins (2006) noted three strong southwesterly flow patterns that are associated with extreme fire weather conditions in the Southwest, and those patterns are captured by our SOMs. Specifically, MT {11} is similar to node 10 from Crimmins (2006) and is associated with 11.0% and 14.0% of Busy95_SW and Busy99_SW days respectively (Table 4). Several MTs {1, 17-18} are rarely associated (< 1%) with either busy threshold and those three MTs are distinct compared to each other (Figure 3; Table 4).

5. Discussion

Busy days and events across the SWA are generally associated with latitudinally-suppressed upper-tropospheric ridging (subtropical ridge axis in western/northwestern Mexico) (e.g., MTs {4, 8, 12}), southwest flow with higher 500 hPa geopotential heights (e.g., MT {11}), or latitudinally-amplified ridging (subtropical ridge axis in SWA) (e.g., MTs

{16, 19-20}. The suppressed ridge and southwest flow with higher geopotential heights MTs (Figure 3 {4, 8, 12}) have PW values of 10-25 mm across most of the SWA, but deeper moisture is confined farther south in Mexico (Figure 4 {4, 8, 12}). Due to the complex terrain in the SWA and northern Mexico, mid-tropospheric (700-400 hPa) moisture often arrives before lower-tropospheric moisture. Additionally, MTs {4, 8, 11-12} depict atmospheric flow that would be less conducive for lower-tropospheric moisture advection from the Gulf of California into the SWA compared to MTs {16, 19-20} (Figures 3-4, 6). Strong diurnal heating and upslope flow can create a deeply-mixed boundary layer and thermally induced circulations that can utilize increased mid-tropospheric moisture and produce thunderstorms (Hales, 1977). With lower-tropospheric moisture confined farther south, an environment conducive for dry thunderstorms develops with characteristic inverted-v soundings where a dry sub-cloud layer and high LCL forms an inverted-v between the dewpoint and temperature profiles (Figure 6; Figures 3-4 {4, 8, 11-12}) (Table 4) (Hall, 2007; Wallmann *et al.,* 2011; Nauslar *et al.,* 2013). Transient upper-tropospheric shortwave troughs and easterly waves also act to increase buoyancy and augment coverage of thunderstorms by lowering heights and temperatures aloft.

MTs with amplified ridging over the SWA also have higher PW values and more LS across the SWA (Figures 3-4 {15-16, 18-20}; Table 2). As the ridge builds northward over the SWA, easterly and southerly flow transports moisture from the Gulf of Mexico across northern Mexico and into the SWA. Additionally, southerly flow increases lower-

tropospheric moisture advection from the Gulf of California into the SWA. The increased moisture creates a more unstable atmosphere and helps trigger thunderstorms beyond the typical terrain-favored locations (e.g., Mogollon Rim and Southern Rockies) (Gebremichael *et al.,* 2007; Gochis and Higgins, 2007; Nesbitt *et al.,* 2008). MTs {15-16, 18-20} that are characterized by amplified ridging are most associated with onset and often occur in July and August when the NAM typically begins and matures. However, MTs {16, 19-20} also often correspond to busy days (Figures 3-4). This could be due to the increased amount and spatial coverage of lightning (Table 4), which enhance ignition potential across a broader area. Enhanced lightning also likely increases fire activity across multiple PSAs given the presence of receptive fuels. Both outcomes strain wildfire suppression resources. Furthermore, MTs {16, 19-20} are more likely to help produce busy wildfire days and events if they occur earlier in the season (e.g., before onset). At this time, peak fuel dryness could offset the increase of atmospheric moisture to help produce the most active part of the wildfire season. The term 'Firesoon' has been used to describe these early moisture intrusions due to their propensity for triggering thunderstorms that ignite wildfires (Brown 2002). Not coincidentally, 3.8% of wildfires in June become large while only 1.9% of wildfires in July become large (Table 6). Additionally, 75.6% of busy events occur before 1 July and 83.9% of all busy days occur before onset (Table 7). Wildfires, especially large wildfires, that begin well before onset strain wildfire suppression resources because they are likely to continue growing until the NAM becomes established.

While associating MTs with busy days and events is important, the atmospheric patterns that precede and follow those days are equally important. Each MT represents a climatology of similar atmospheric patterns that typically occur from April through September across the SWA. By analyzing MTs assigned to specific days around busy days and events, observations and inferences about the progression of atmospheric patterns (e.g., MTs) can be gleaned. Four general atmospheric pattern progressions emerge when examining MTs around busy days and events for the SWA: 1) zonal or southwest flow transition to ridging; 2) variation between suppressed and amplified ridging over the SWA; 3) zonal or southwest flow transitioning to ridging followed by a return to zonal or southwest flow; and 4) ridging over the SWA with the ridge axis exhibiting east-west movement (Figure 7).

The MT progressions around busy days and events usually occur on timescales of days to weeks. This underscores the importance of progressive wave patterns characterized by alternating upper-tropospheric troughs and ridges. MTs with upper-tropospheric troughing and zonal or southwesterly flow over the SWA have lower PW values and tighter height gradients across the SWA. These conditions translate to dry and windy surface conditions that help cure fuels and promote a receptive fuel bed for wildfire ignition and spread. The MTs characterized by upper-tropospheric ridging and higher 500 hPa geopotential heights are associated with higher LS and PW values across the SWA. Higher 500 hPa geopotential heights are also indicative of warmer surface temperatures.

This variation between periods of hot, dry, and windy surface conditions and increased moisture and lightning appears to drive much of the fire weather and occurrence across the SWA. Specifically, MT progressions that represent a transition from upper-tropospheric ridging to troughing are reminiscent of the breakdown of the upper-tropospheric ridge, a known critical fire weather pattern (Werth *et al.* 2011). The breakdown involves decreasing geopotential heights with an eastward or equatorward shift of the ridge axis that can lead to the following pattern change: 1) hot and dry surface conditions; 2) increasing atmospheric instability and moisture leading to thunderstorms; and 3) dry and windy surface conditions. That progression is conducive for large wildfire occurrence as lightning occurs with receptive fuels, which is followed by dry and windy conditions that promote fire spread. The periodicity of these patterns varies, and future work could entail examining the duration and frequency of these patterns more closely.

Holdovers are wildfires that are ignited but remain small (i.e., single tree) until favorable atmospheric conditions develop and subsequently promote fire growth. A wildfire's discovery date and its ignition date may not match, and holdovers are difficult to quantify and predict (Anderson, 2002). Holdovers and large wildfire growth after the discovery date introduce errors into our analysis. However, utilizing the busy day and event thresholds mitigate some of these issues because these consider relatively rare events (< 5% of occurrence) and deemphasize total acres burned. Future work could use the Monitoring Trends in Burn Severity database to calculate area burned on a daily

timescale and apply the same rigorous atmospheric pattern and fuel indices analysis. However, such an analysis would be confined to examining only larger wildfires due to the spatial resolution and accuracy of this database (Kolden *et al.,* 2012).

The methods implemented in this analysis produce realistic and meaningful annual NAM onset dates by PSA. This helps frame wildfire occurrence in the SWA. Generally, onset progresses from east to west and south to north across the SWA, but with large interannual variability. The differences in the onset dates between Arizona and western New Mexico from eastern New Mexico and west Texas could be attributed to a precipitation dipole that exists between the Plains (central U.S.) and the mountainous Southwest (Figure 5; Higgins *et al.,* 1997; Higgins *et al.,* 1999; Mitchell *et al.,* 2002; Adams and Stensrud, 2007; Stensrud, 2013). MTs {15-16, 18-20} are most associated with the NAM onset and depict southerly flow over most of the SWA and a northward shift of easterlies over northern Mexico leading to increased lightning and PW across the SWA (Figures 3-4 {15-16, 18-20}) (Table 4). These MTs are very similar to the SOM nodes that Cavazos *et al.,* (2002) found to be most associated with wet NAM modes for southeast Arizona (or "bursts," as in Carleton, (1986) and Watson *et al.,* (1994)). MT {17} is curiously unrelated to NAM onset, but 500 hPa heights are lower than other MTs associated with onset, and the ridge axis is shifted west limiting moisture advection from the Gulf of California. This induces drier west-northwest flow over most of the Southwest, which confirms prior research (Table 4) (Carleton 1986; Carleton *et al.,* 1990; Higgins *et al.,* 1999; Cerezo-Mota *et al.,* 2011).

6. Conclusions

Using atmospheric reanalysis data, gridded surface weather observations, and historical wildfire datasets we demonstrated that the most frequently occurring synoptic patterns before and during the NAM modulate large wildfire occurrence. Several MTs or MT progressions are associated with significant wildfire episodes (i.e., busy days or events) (Figure 7):

- Zonal or southwest flow transition to ridging
- Fluctuation between suppressed and amplified ridging over the SWA
- Zonal or southwest flow transitioning into ridging followed by a return to zonal or southwest flow
- Variation between suppressed and amplified ridging over the SWA with the ridge axis exhibiting east-west movement

If these patterns develop before the NAM onset, and thus coincide with peak fuel and atmospheric dryness, then the likelihood of significant wildfire episodes increases. A method for determining the NAM onset by PSA as directly related to wildfire was also established corresponding to observed, and to some extent predictable, atmospheric patterns that promote increased moisture and lightning. We provided novel results documenting MTs directly associated with significant wildfire episodes and NAM onset in the SWA.

The results of this work are intended to provide decision support information and improve understanding of atmospheric processes associated with NAM and their impact on wildfire activity. Improved understanding of this association may benefit operational fire meteorologists and managers by providing identifiable atmospheric patterns associated with increased wildfire activity that are particularly impactful on suppression resources and can lead to overall improvements in planning and logistical strategies (Ray *et al.,* 2007).

Acknowledgements

We would like to thank the USDA Forest Service for providing the funding (10-CS-11130206-047), and Vaisala for allowing the use of lightning data for wildfire applications. We would also like to thank Chuck Maxwell, John Saltenberger, and Terry Marsha for their input and advice for the paper. Finally, we would like to thank David Reusch and Michael Crimmins for their expertise and help on SOMs, John Abatzolgou for helping obtain and organize the METDATA, and Andrew Joros for helping obtain and organize the NARR dataset. We would also like to thank the two anonymous reviewers for their thorough and constructive comments, which greatly improved the manuscipt.

References

Abatzoglou JT, Brown TJ. 2009. Influence of the Madden–Julian Oscillation on summertime cloud-to-ground lightning activity over the continental United States. *Mon. Wea. Rev.* **137:** 3596-3601.

Abatzoglou JT. 2013. Development of gridded surface meteorological data for ecological applications and modelling. *Int. J. Climatol.* **33**: 121-131.

Adams DK, Comrie AC. 1997. The North American Monsoon. *Bull. Amer. Meteor. Soc.* **78:** 2197-2213.

Adams JL, Stensrud DJ. 2007. Impact of tropical easterly waves on the North American Monsoon. *J. Climate* **20**: 1219-1238.

Anderson K. 2002. A model to predict lightning-caused fire occurrences. *Int. J. Wildland Fire* **11**: 163-172.

Barlow M, Nigam S., Berbery EH. 1998. Evolution of the North American Monsoon system. *J. Climate* **11**: 2238-2257.

Becker EJ, Berbery EH, Higgins RW. 2009. Understanding the Characteristics of Daily Precipitation over the United States Using the North American Regional Reanalysis. *J. Climate* **22**: 6268–6286.

Brandt RR. 2006. The North American Monsoon system in southern Arizona. Dissertation, Department of Geography and Regional Development, University of Arizona, 130 pp.

Brown TJ. 2002. The North American "Firesoon". In report on research opportunities for climate and society interactions in the North American Monsoon region, Workshop on Applications and Human Dimensions of Monsoon Research, 18-20 June 2001, Tucson, AZ, A.J Ray and R.S. Webb (Eds.), Report for NOAA OAR, 64 pp.

Bryson, RA and Lowry, WP. 1955. Synoptic climatology of the Arizona summer precipitation singularity. *Bull. Amer. Meteor. Soc.,* **36**: 329-339.

Carleton AM. 1986. Synoptic-dynamic character of “bursts” and “breaks” in the southwest U.S. summer precipitation singularity. *J. Climatol.* **6**: 605–623.

Carleton AM, Carpenter DA, Weser PJ. 1990. Mechanisms of interannual variability of the southwest United States summer rainfall maximum. *J. Climate* **3**: 999-1015.

Cavazos T, Comrie AC, Liverman DM. 2002. Intraseasonal variability associated with wet monsoons in southeast Arizona. *J. Climate* **15**: 2477-2490.

Cerezo-Mota R, Allen M, Jones R. 2011. Mechanisms controlling precipitation in the northern portion of the North American Monsoon. *J. Climate* **24:** 2771-2783.

Crimmins MA, Comrie AC. 2005. Interactions between antecedent climate and wildfire variability across southeastern Arizona. *Int. J. Wild- land Fire* **13**: 455-466.

Crimmins MA. 2006. Synoptic climatology of extreme fire-weather conditions across the southwest United States. *Int. J. Climatol*. **26**: 1001–1016.

Dominguez, F Kumar P. 2008. Precipitation Recycling Variability and Ecoclimatological Stability—A Study Using NARR Data. Part I: Central U.S. Plains Ecoregion. *J. Climate* **21**: 5165–5186.

Dominguez F, Kumar P, Vivoni ER. 2008. Precipitation recycling variability and ecoclimatological stability—a study using NARR data. Part II: North American Monsoon region. *Journal of Climate* **21**: 5187-5203.

Doubler DL, Winkler JA, Bian X, Walters CK, Zhong S. 2015. An NARR-derived climatology of southerly and northerly low-level jets over North America and coastal environments. *J. Appl. Meteor. Climatol.* **54**: 1596–1619.

Douglas MW, Maddox RA, Howard K, Reyes S. 1993. The Mexican monsoon. *J. Climate* **6**: 1665- 1677.

Dowdy AJ, Mills GA. 2012. Atmospheric and fuel moisture characteristics associated with lightning-attributed fires. *J. Appl. Meteor. Climatol*. **51**: 2025–2037.

Earth System Research Laboratory Physical Sciences Division (ESRL PSD). 2014. Multivariate ENSO Index (MEI). http://www.esrl.noaa.gov/psd/enso/mei/index.html.

Ellis, A. W., E. M. Saffell, and T. W. Hawkins, 2004: A method for defining monsoon onset and demise in the southwestern USA. Int. J. Climatol., 24, 247–265.

Evett RR, Mohrle CR, Hall BL, Brown TJ, Stephens SL. 2008. The effect of monsoonal atmospheric moisture on lightning wildfire ignitions in southwestern North America. *Agric. Forest Meteorol.* **148**: 1478-1487.

Favors JE, Abatzoglou JT. 2012. Regional surges of monsoonal moisture into the southwestern United States. *Mon. Wea. Rev.* **141**: 182-191.

Gebremichael M, Vivoni ER, Watts CJ, Rodríguez JC. 2007. Submesoscale spatiotemporal variability of North American monsoon rainfall over complex terrain. *J. Climate* **20**: 1751-1773.

Gochis DJ, Higgins RW. 2007. The path to improving predictions of the North American Monsoon. *Newsletter, U.S. CLIVAR Variations* **5**.

Grantz K, Rajagopalan B, Clark M, Zagona E. 2007. Seasonal shifts in the North American Monsoon. *J. Climate* **20:** 1923-1935.

Hales, JE. 1977. On the relationship of convective cooling to nocturnal thunderstorms at Phoenix. *Mon. Wea. Rev.* **105**: 1609-1613.

Hall BL. 2007. Precipitation associated with lightning-ignited wildfires in Arizona and New Mexico. *Int. J. Wildland Fire* **16**: 242-254.

Hawkins TW, Ellis AW, Skindlov JA, Reigle D. 2002. Intra-annual analysis of the North American snow cover–monsoon teleconnection: Seasonal forecasting utility. *J. Climate*, **15**: 1743-1753.

Hendon HH, Sperber KR, Waliser DE, Wheeler MC. 2011. Modeling monsoon intraseasonal variability: From theory to operational forecasting. *Bull. Amer. Meteor. Soc.* **92**: ES32–ES35.

Hewitson BC, Crane RG. 2002. Self-organizing maps: Applications to synoptic climatology. *Climate Research* **22**: 13–26.

Higgins RW, Yao Y, Wang XL. 1997. Influence of the North American Monsoon system on the U.S. summer precipitation regime. *J. Climate* **10**: 2600-2622.

Higgins RW, Mo KC, Yao Y. 1998. Interannual variability of the U.S. summer precipitation regime with emphasis on the Southwestern Monsoon. *J. Climate* **11**: 2582-2606.

Higgins RW, Chen Y, Douglas AV. 1999. Interannual variability of the North American warm season precipitation regime. *J. Climate* **12**: 653-680.

Kohonen T. 2001: *Self-Organizing Maps*. Springer-Verlag, 503 pp.

Kolden CA, Lutz JA, Key CH, Kane JT, van Wagtendonk JW. 2012. Mapped versus actual burned area within wildfire perimeters: Characterizing the unburned *Forest Ecol. Manage.* **286**: 38–47.

Lo F, Clark MP. 2002. Relationships between spring snow mass and summer precipitation in the southwestern United States associated with the North American Monsoon system. *J. Climate* **15**: 1378-1385.

Mathworks. 2017. Self-Organizing Maps. https://www.mathworks.com/help/nnet/self-organizing-maps.html

Means JD. 2012. GPS Precipitable Water as a Diagnostic of the North American Monsoon in California and Nevada. *J. Climate* **26**: 1432-1444.

Mejia JF, Douglas MW, Lamb PJ. 2015. Observational investigation of relationships between moisture surges and mesoscale to large-scale convection during the North American Monsoon. *Int. J. Climatol*. **36**: 2555–2569.

Mesinger F, Coauthors. 2006. North American Regional Reanalysis. Bulletin of the A.M.S. **87**: 343-360.

Mitchell DL, Ivanova D, Rabin R, Brown TJ, Redmond K. 2002. Gulf of California sea surface temperatures and the North American Monsoon: Mechanistic implications from observations. *J. Climate* **15**: 2261-2281.

Mohrle CR. 2003. The Southwest Monsoon and relation to fire occurence. M.S. thesis, Department of Physics/Division of Atmospheric Sciences (DRI), University of Nevada, Reno, 97 pp. Online at http://www.cefa.dri.edu/Publications/charliethesis.pdf.

National Weather Service Weather Forecast Office Tucson. 2015. Monsoon Information Index, 12 November 2015. [Available online at: http://www.wrh.noaa.gov/twc/monsoon/monsoon_info.php].

Nauslar NJ, Kaplan ML, Wallmann J, Brown TJ. 2013. A forecast procedure for dry thunderstorms. *J. Operational Meteor.* **1**: 200–214.

Nesbitt SW, Gochis DJ, Lang TJ. 2008. The diurnal cycle of clouds and precipitation along the Sierra Madre Occidental observed during NAME-2004: Implications for warm season precipitation estimation in complex terrain. *J. Hydrometeor.* **9**: 728-743.

Newman A, Johnson RH. 2012. Mechanisms for Precipitation Enhancement in a North American Monsoon Upper-Tropospheric Trough. *J. Atmos. Sci.* **69**: 1775–1792.

Pascale, S and Bordoni, S. 2016. Tropical and Extratropical Controls of Gulf of California Surges and Summertime Precipitation over the Southwestern United States. Mon. Wea. Rev., 144, 2695-2718, https://doi.org/10.1175/MWR-D-15-0429.1

Radhakrishna B, Fabry F, Braun JJ, Van Hove T. 2015. Precipitable water from GPS over the continental United States: Diurnal cycle, intercomparisons with NARR, and link with convective initiation. *J. Climate* **28**: 2584–2599.

Ray AJ, Garfin GM, Wilder M, Vásquez-León M, Lenart M, Comrie AC. 2007. Applications of monsoon research: Opportunities to inform decision making and reduce regional vulnerability, *J. Climate* **20**: 1608-1627.

Reiter ER, Tang M 1984. Plateau effects on diurnal circulation patterns. *Mon. Wea. Rev.* **112**: 638–651.

Reusch DB, Alley RB, Hewitson BC. 2005. Relative performance of self-organizing maps and principal component analysis in pattern extraction from synthetic climatological data. *Polar Geogr.* **29**: 227 – 251.

——, ——, —— 2007. North Atlantic climate variability from a self-organizing map perspective, *J. Geophys. Res.* **112**: D02104.

Reusch DB. 2011. Nonlinear climatology and paleoclimatology: Capturing patterns of variability and change with self-organizing maps, *Physics and Chemistry of the Earth* **35**: 329-340.

Rodriguez-Iturbe I, D'Odorico P, Rinaldo A. 1998, Possible self-organizing dynamics for land–atmosphere interaction. *J. Geophys. Res.* **103D:** 23 071–23 077.

Sammon JW. 1969. A nonlinear mapping for data structure analysis. *IEEE Transactions on Computers* **18**: 401–409.

Seastrand S, Serra Y, Castro C, Ritchie E. 2015. The dominant synoptic-scale modes of North American monsoon precipitation. *Int. J. Climatol*. **35**: 2019–2032.

Short KC. 2015. Spatial wildfire occurrence data for the United States, 1992-2013 [FPA_FOD_20150323]. 3rd Edition. Fort Collins, CO: Forest Service Research Data Archive.

Stensrud, S. J. 1996. Importance of low-level jets to climate: A review, *J. Clim*., **9**, 1698‑1711, doi:10.1175/15200442(1996)009<1698:IOLLJT.2.0.CO;2.

Stensrud DJ, Gall RL, Nordquist MK. 1997. Surges over the Gulf of California during the Mexican Monsoon. *Mon. Wea. Rev.* **125**: 417-437.

Stensrud DJ. 2013. Upscale effects of deep convection during the North American Monsoon. *J. Atmos. Sci*. **70**: 2681–2695.

Swales D, Alexander M, Hughes M. 2016. Examining moisture pathways and extreme precipitation in the U.S. Intermountain West using self-organizing maps, *Geophys. Res. Lett*. **43**: 1727–1735.

Tang M, Reiter ER. 1984. Plateau monsoons of the Northern Hemisphere: A comparison between North America and Tibet. *Mon. Wea. Rev*. **112**: 617-637.

Turrent C, Cavazos T. 2012. A numerical investigation of wet and dry onset modes in the North American Monsoon core region. Part I: A regional mechanism for interannual variability. *J. Climate* **25**: 3953–3969.

Vera C, Coauthors. 2006. Toward a unified view of the American Monsoon systems. *J. Climate* **19**: 4977-5000.

Wallmann J, Milne R, Smallcomb C, Mehle M. 2010. Using the 21 June 2008 California lightning outbreak to improve dry lightning forecast procedures. *Wea. Forecasting* **25**: 1447-1462.

Watson AI, Holle RL, López RE. 1994. Cloud-to-ground lightning and upper-air patterns during bursts and breaks in the Southwest Monsoon. *Mon. Wea. Rev* **122**: 1726-1739.

Werth PA, Potter BE, Clements CB., Finney MA, Goodrick, SL, Alexander ME, Cruz MG, Forthofer JA, McAllister SS. 2011. Synthesis of Knowledge of Extreme Fire Behavior: Volume I for Fire Managers. Gen. Tech. Rep. PNW-GTR-854. Portland, OR: US Department of Agriculture, Forest Service, Pacific Northwest Research Station.

Westerling AL, Brown TJ, Gershunov A., Cayan DR, Dettinger MD. 2003. Climate and Wildfire in the Western United States. Bull. Amer. Met. Soc. **84**(5): 595-604

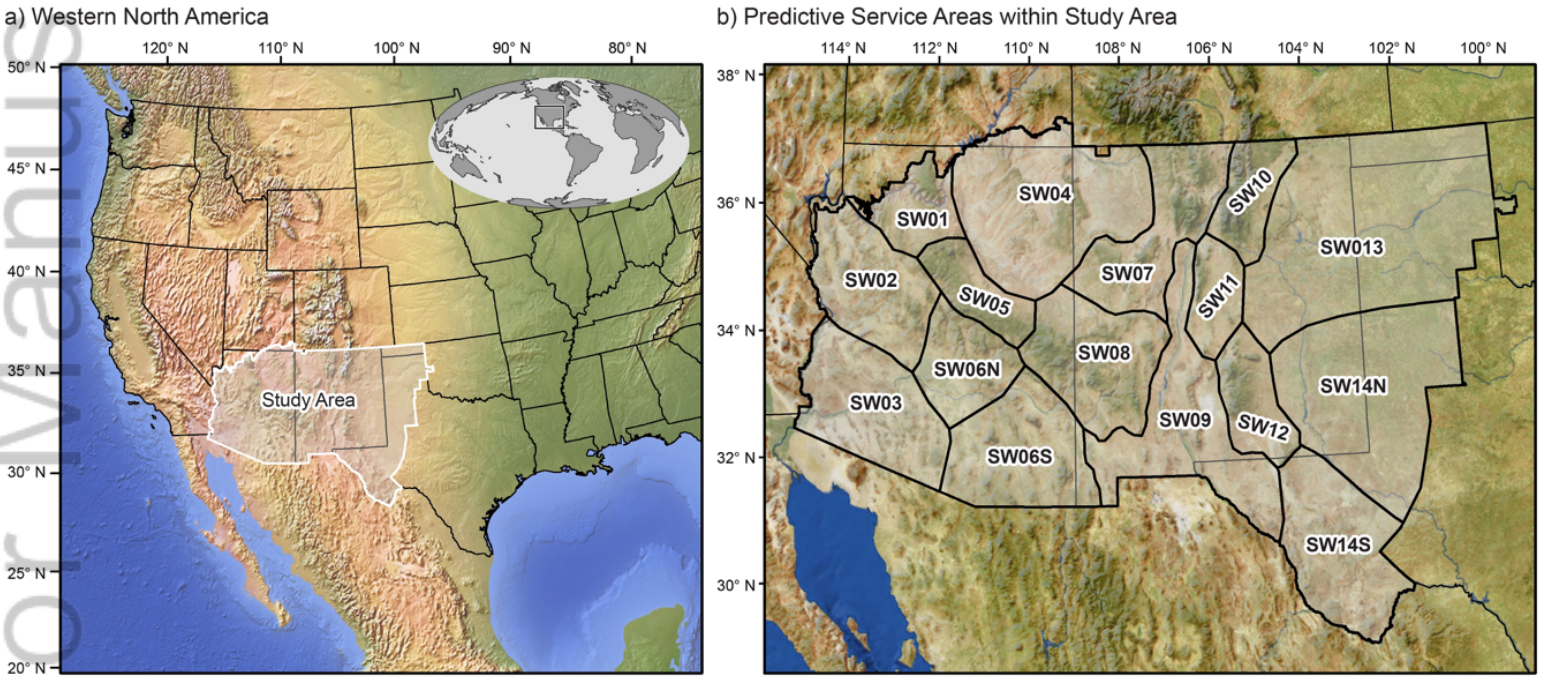

Figure1.tiff

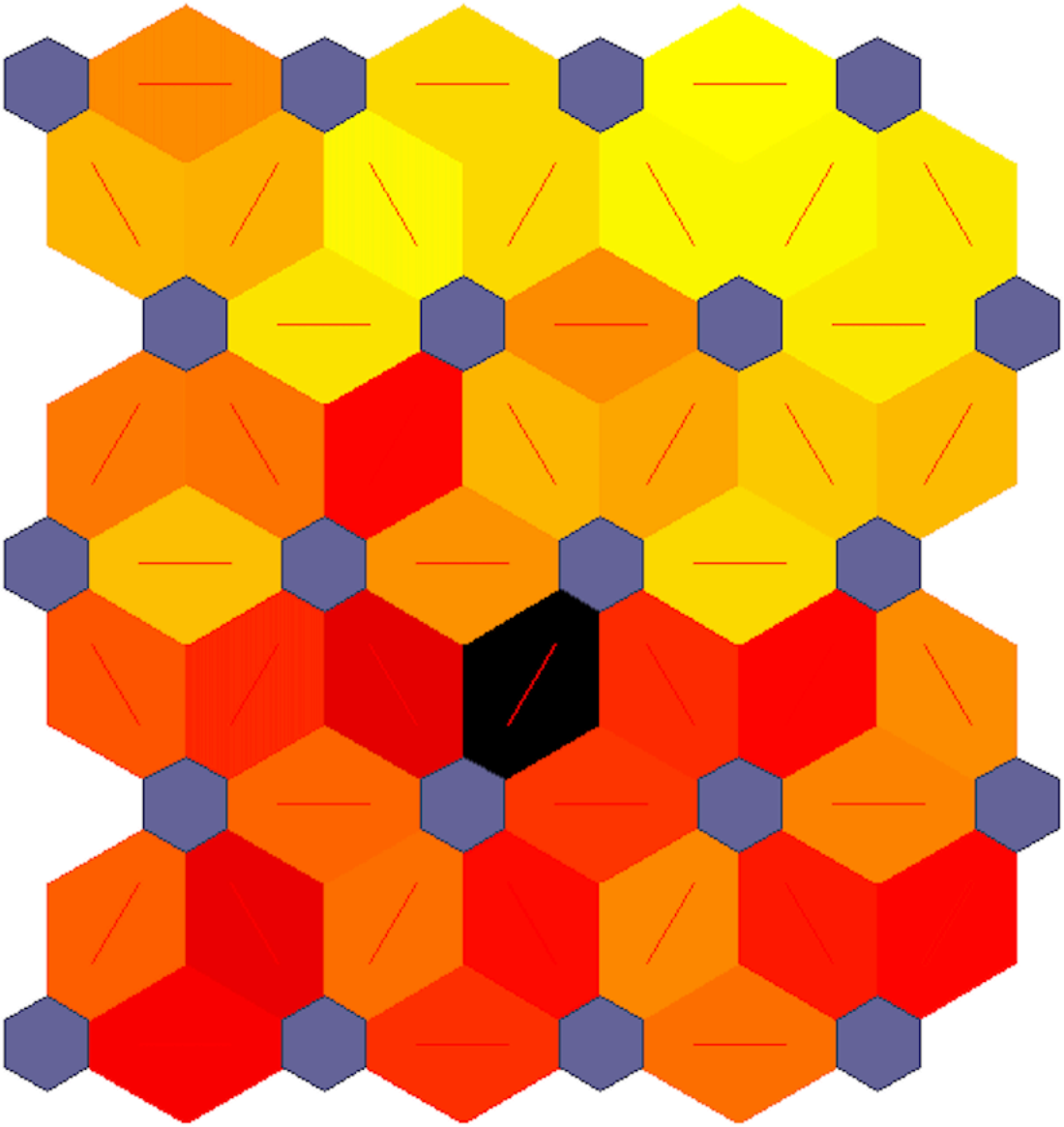

Figure2.tiff

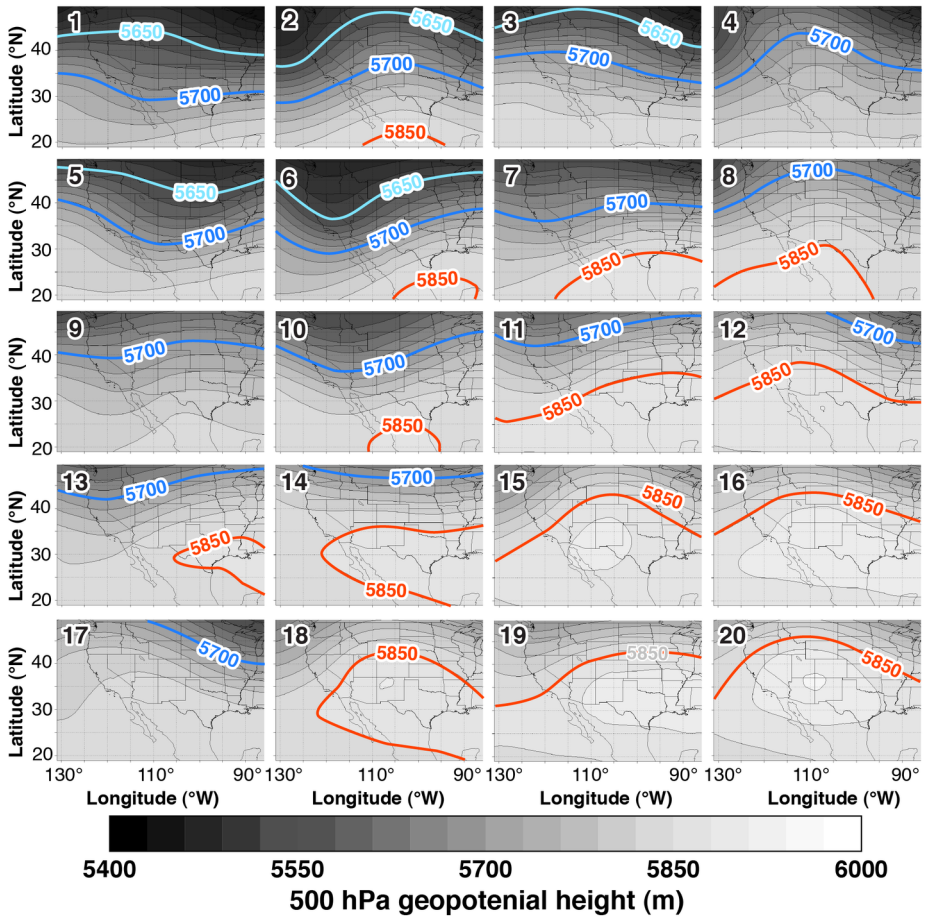

Figure3.tiff

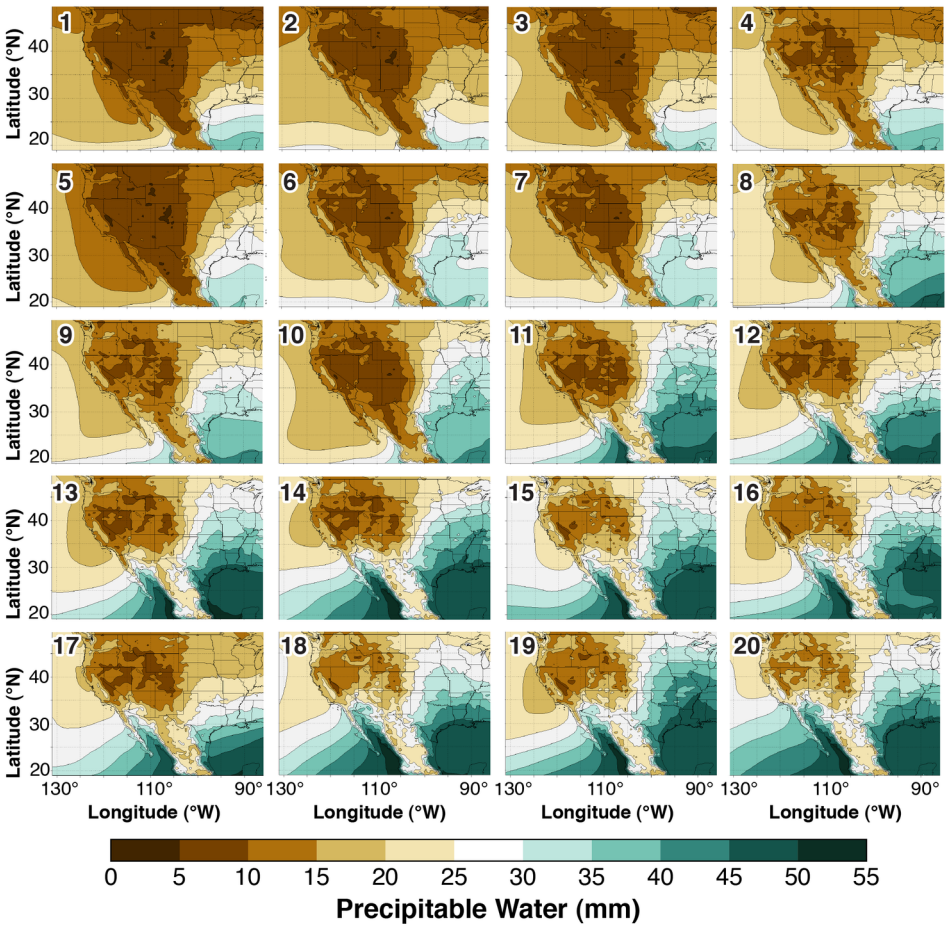

Figure4.tiff

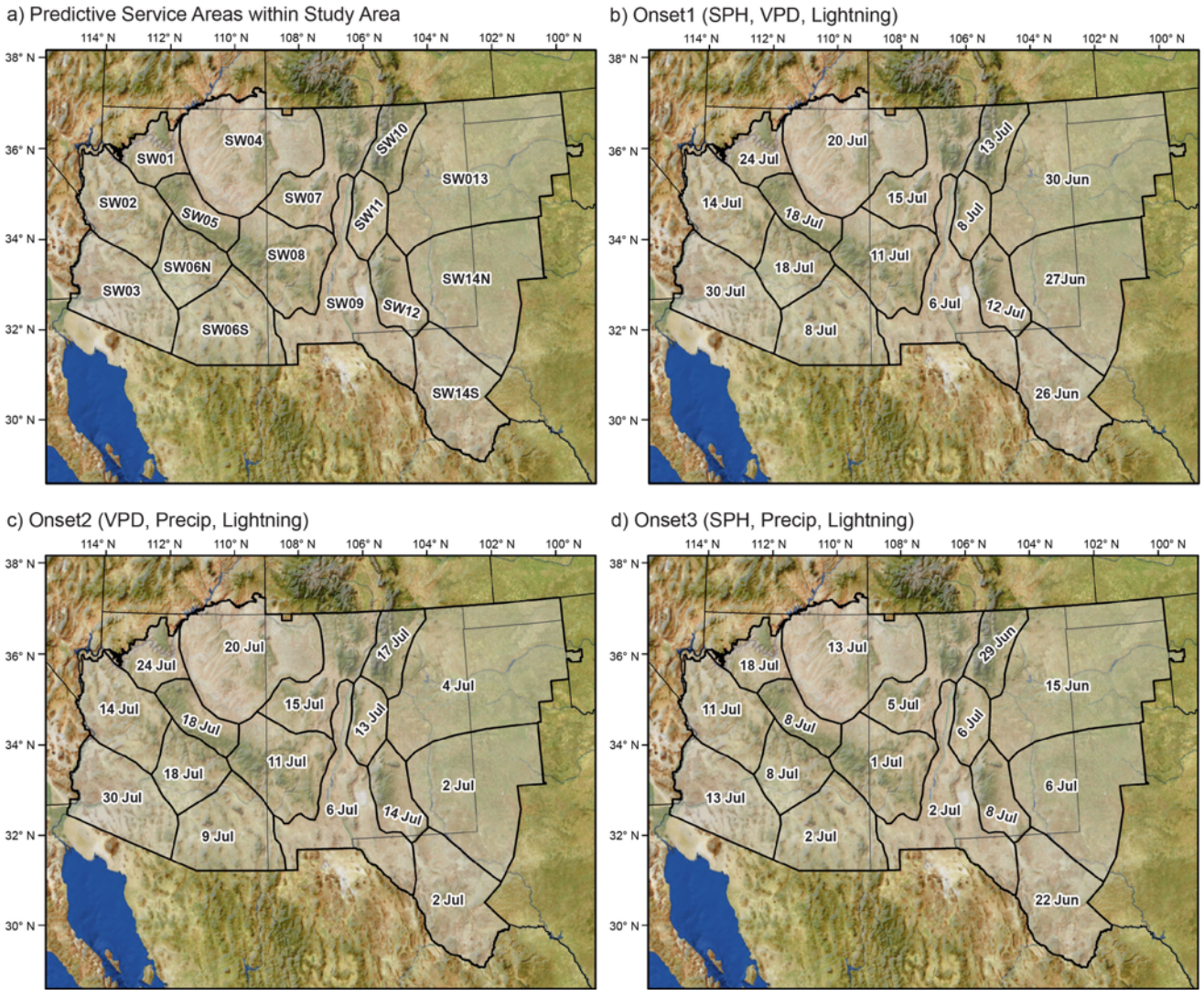

Figure5.tiff

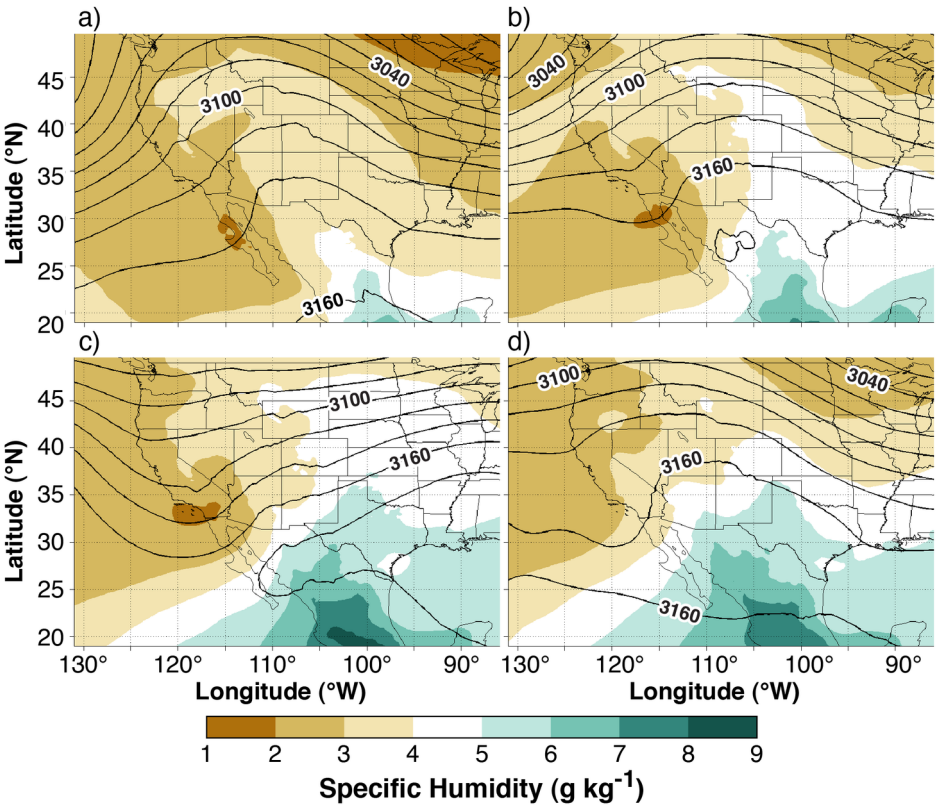

Figure6.tiff

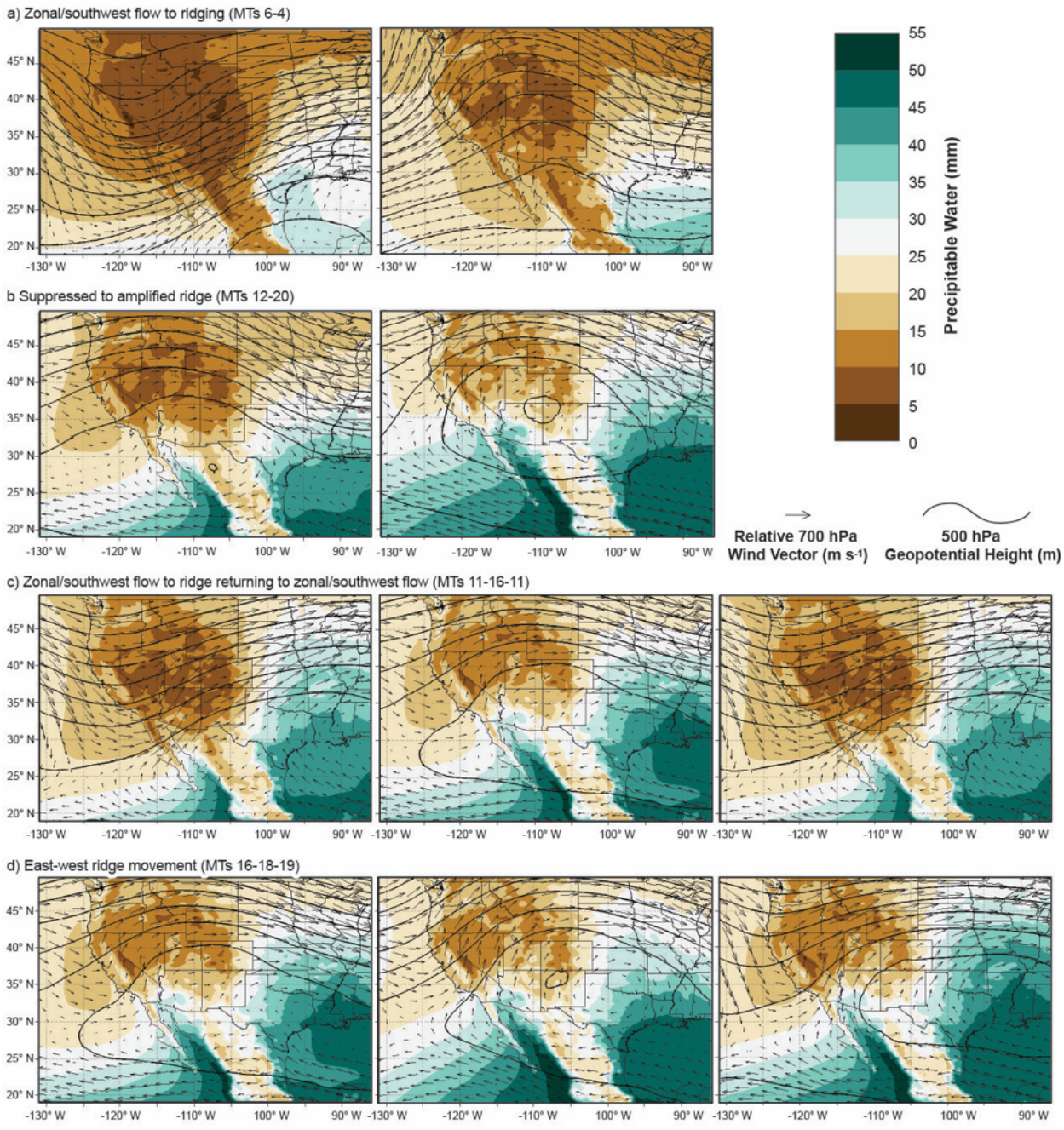

Figure7.tiff

Impact of the North American Monsoon on wildfire activity in the southwest United States

Nicholas J. Nauslar*, Benjamin J. Hatchett, Timothy J. Brown, Michael L. Kaplan, and John F. Mejia

Wildfire activity in the southwest United States is inextricably linked with the timing and strength of the North American Monsoon (NAM). Using synoptic classification techniques, certain atmospheric patterns were associated with significant wildfire episodes and the NAM onset in the southwest United States. Identifying atmospheric patterns pertinent to significant wildfire episodes in the SWA would aid operational fire meteorologists in better prediction of significant wildfire episodes and provide lead time to fire managers more efficiently allocate firefighting resources.

Table 1: Large wildfire threshold for each PSA in the SWA as determined by Southwest PS.

PSA	Large Wildfire Threshold (Acres)
SW01	100
SW02	300
SW03	300
SW04	100
SW05	50
SW06S	100
SW06N	500
SW07	100
SW08	300
SW09	300
SW10	100
SW11	100
SW12	100
SW13	2000
SW14	200
SW14N	2000

Table 4: Showing the percentage of occurrence for each map type (MT) for all days, Busy95_SW, Busy99_SW, and Onset1 days and the median lightning strikes (LS) decile (Dec) for each MT.

	Count	All Days	Busy95_SW	Busy99_SW	Onset1	Median LS Decile
MT1	135	3.4%	0.5%	0.0%	0.0%	1
MT2	122	3.0%	2.3%	3.5%	0.0%	1
MT3	141	3.5%	2.7%	1.8%	0.0%	1
MT4	120	3.0%	6.4%	8.8%	0.0%	3
MT5	139	3.5%	2.3%	1.8%	0.0%	1
MT6	136	3.4%	2.7%	3.5%	0.0%	1
MT7	190	4.7%	4.1%	3.5%	0.0%	2
MT8	179	4.4%	5.5%	5.3%	1.8%	4
MT9	186	4.6%	3.2%	3.5%	0.7%	4
MT10	174	4.3%	2.7%	1.8%	0.0%	2
MT11	228	5.7%	11.0%	14.0%	2.8%	4
MT12	207	5.1%	8.2%	10.5%	3.9%	5
MT13	237	5.9%	2.7%	5.3%	8.5%	4
MT14	230	5.7%	2.7%	5.3%	6.0%	5
MT15	239	5.9%	5.0%	1.8%	9.9%	6
MT16	285	7.1%	12.8%	7.0%	19.0%	8
MT17	206	5.1%	2.3%	0.0%	1.4%	3
MT18	254	6.3%	3.2%	0.0%	12.3%	6
MT19	342	8.5%	9.6%	10.5%	18.7%	7

Table 5: Mean number of wildfires per year for the SWA by type and size for 1992-2013.

Total Wildfires Per Year	4064
Total Large Wildfires Per Year	108
Lightning Caused Wildfires Per Year	1972
Lightning Caused Large Wildfires Per Year	62
Human Caused Wildfires Per Year	2092

Table 6: Total SWA wildfires by type and month for 1992-2013.

	Wildfires	Large Wildfires	Lightning-Caused Wildfires	Lightning-Caused Large Wildfires	Human Wildfires	Human-Caused Large Wildfires
April	8318	300	744	67	7574	233
May	14789	417	3348	151	11441	266
June	21443	822	8774	476	12669	346
July	25687	496	17367	375	8320	121
August	13899	267	10545	229	3354	38

Table 7: Displaying the number (Count) of occurrences for each type of event from 1992-2013. Also shows the percentage of events that transpired before onset (if applicable) and before 1 July. Shows number of occurrences for each type of event by month.

	Count	% Before Onset	% Before 1 July	April	May	June	July	August	September
Busy95_PSA	298	85.23%	62.4%	28	40	118	76	33	3
Busy99_PSA	292	82.53%	55.1%	25	31	105	98	30	3
Busy95_SW	219		66.2%	23	31	91	51	22	1
Busy99_SW	57		77.2%	6	10	28	11	2	0
Event_ 2_95	108		70.4%	13	19	44	24	8	0
Event_3_95	83		72.3%	8	17	35	17	6	0
Event_7_95	49		73.5%	6	7	23	11	2	0
Event_10_95	36		77.8%	3	8	17	7	1	0
Event_2_99	27		81.5%	2	5	15	5	0	0
Event_3_99	17		88.2%	1	4	10	2	0	0
Event_7_99	11		81.8%	0	2	7	2	0	0
Event_10_99	10		80.0%	0	2	6	2	0	0

Table 8: Displays the number of times a PSA had at least one large wildfire when the Busy99_PSA or Busy95_PSA threshold was exceeded. Also shows the percentage representing the proportion for each PSA when having at least one large wildfire when the Busy99_SW or Busy95_SW threshold was exceeded.

	SW01	SW02	SW03	SW04	SW05	SW06S	SW06N	SW07	SW08	SW09	SW10	SW11	SW12	SW13	SW14S	SW14N
Busy99_SW	7	20	4	6	14	39	15	6	23	12	8	9	28	11	13	13
	12.3%	35.1%	7.0%	10.5%	24.6%	68.4%	26.3%	10.5%	40.4%	21.1%	14.0%	15.8%	49.1%	19.3%	22.8%	22.8%
Busy95_SW	24	46	14	16	42	120	47	22	70	25	27	18	61	31	38	31
	11.0%	21.0%	6.4%	7.3%	19.2%	54.8%	21.5%	10.0%	32.0%	11.4%	12.3%	8.2%	27.9%	14.2%	17.4%	14.2%

Table 2: Map type (MT) occurrence by month summed for the period of 1995-2013 and associated median lightning strike (LS) total decile..

	April	May	June	July	August	September	Median LS Decile
MT1	134	1	0	0	0	0	1
MT2	104	18	0	0	0	0	1
MT3	98	43	0	0	0	0	1
MT4	54	64	2	0	0	0	3
MT5	103	36	0	0	0	0	1
MT6	107	29	0	0	0	0	1
MT7	35	137	15	0	0	3	2
MT8	1	93	79	0	0	6	4
MT9	16	124	33	0	0	13	4
MT10	8	106	51	0	0	9	2
MT11	0	7	164	19	8	30	4
MT12	0	4	76	17	27	83	5
MT13	0	4	88	12	7	126	4
MT14	0	0	29	55	70	76	5
MT15	0	0	34	83	86	36	6
MT16	0	0	34	146	97	8	8
MT17	0	16	29	1	0	160	3
MT18	0	0	14	52	110	78	6
MT19	0	0	8	170	145	19	7

Table 3: Median, inter-quartile range (IQR; number of days), median absolute deviation (MAD; number of days), 10th percentile onset date, and 90th percentile onset day-of-year (DOY) by PSA for the three onset metrics using specific humidity (q), vapor pressure deficit (VPD), precipitation (precip), and lightning strikes (LS) from 1995-2013.

	SW01	SW02	SW03	SW04	SW05	SW06S	SW06N	SW07	SW08	SW09	SW10	SW11	SW12	SW13	SW14S	SW14N
Onset1 (q, VPD, LS)	24-Jul	14-Jul	30-Jul	20-Jul	18-Jul	8-Jul	18-Jul	15-Jul	11-Jul	6-Jul	13-Jul	8-Jul	12-Jul	30-Jun	26-Jun	27-Jul
IQR	35	25	32	19	19	10	19	21	15	17	29	25	26	21	34	52
MAD	17	10	14	10	10	6	11	11	8	7	13	13	14	11	11	19
90th	21-Aug	11-Aug	30-Aug	12-Aug	7-Aug	20-Jul	3-Aug	3-Aug	24-Jul	30-Jul	28-Jul	1-Aug	4-Aug	23-Jul	4-Aug	20-Aug
10th	4-Jul	3-Jul	4-Jul	4-Jul	3-Jul	29-Jun	30-Jun	1-Jul	28-Jun	20-Jun	16-Jun	11-Jun	18-Jun	4-Jun	14-Jun	5-Jun
Onset2 (VPD, Precip, LS)	24-Jul	14-Jul	30-Jul	20-Jul	18-Jul	9-Jul	18-Jul	15-Jul	11-Jul	6-Jul	17-Jul	13-Jul	14-Jul	4-Jul	2-Jul	2-Jul
IQR	35	25	32	19	19	10	17	25	16	17	28	20	36	34	39	53
MAD	17	10	14	10	10	6	5	12	8	7	14	10	18	19	16	26
90th	21-Aug	11-Aug	30-Aug	12-Aug	7-Aug	20-Jul	3-Aug	9-Aug	25-Jul	30-Jul	3-Aug	3-Aug	12-Aug	9-Aug	14-Aug	10-Aug
10th	4-Jul	3-Jul	4-Jul	4-Jul	3-Jul	29-Jun	30-Jun	1-Jul	28-Jun	12-Jun	25-Jun	14-Jun	14-Jun	5-Jun	14-Jun	2-Jun
Onset3 (q, Precip, LS)	18-Jul	11-Jul	13-Jul	13-Jul	8-Jul	2-Jul	8-Jul	5-Jul	1-Jul	2-Jul	29-Jun	6-Jul	8-Jul	15-Jun	22-Jun	6-Jul
IQR	20	16	20	18	15	10	15	16	14	11	21	18	32	22	40	37
MAD	12	9	9	9	7	7	8	8	8	7	6	9	13	8	15	20
90th	7-Aug	31-Jul	16-Aug	31-Jul	17-Jul	15-Jul	25-Jul	14-Jul	15-Jul	24-Jul	19-Jul	18-Jul	10-Aug	11-Jul	1-Aug	6-Aug